PCCP

Mechanistic Model for Hydrogen Activation, Spillover, and Its Chemical Reaction in Zeolite-Encapsulated Pt Catalyst

Journal:	*Physical Chemistry Chemical Physics*
Manuscript ID	CP-ART-09-2015-005536.R1
Article Type:	Paper
Date Submitted by the Author:	20-Nov-2015

Complete List of Authors:	Shin, Hyeyoung; Korea Advanced Inst. of Science and Technology, Dept of Chemical and Biomolecular Engineering Choi, Minkee; Korea Advanced Institute of Science and Technology, Department of Chemical and Biomolecular Engineering Kim, Hyungjun; KAIST, Graduate School of EEWS

PCCP

ARTICLE

Mechanistic Model for Hydrogen Activation, Spillover, and Its Chemical Reaction in Zeolite-Encapsulated Pt Catalyst

Hyeyoung Shin,[a] Minkee Choi[b] and Hyungjun Kim*[a]

9Received 00th January 20xx,
Accepted 00th January 20xx

DOI: 10.1039/x0xx00000x

www.rsc.org/

The hydrogen (H) spillover phenomenon has attracted considerable attention in the catalysis field. Many researchers have focused on the phenomenon itself, as well as its applications for advanced catalytic systems. In particular, H spillover on non-reducible materials, such as alumina, silica, and zeolites, is a controversial issue owing to the lack of understanding regarding its mechanistic properties. In this study, we use density functional theory calculations to propose the entire mechanism of H spillover from H_2 activation on platinum to its participation in chemical reactions on the external surface of the zeolites. We determined that surface hydroxyl groups of the zeolites, such as Brønsted acid sites, play a role to initiate the H spillover, and the Lewis acid sites facilitate the entire process by allowing H to be transferred as a H^+/e^- charge pair, as well as providing good binding sites for organic reactants. Theoretical results explain key experimental features, and we expect that this work will help to elucidate the H spillover phenomenon on non-reducible support materials and to utilize it for catalytic systems.

1. Introduction

Hydrogen (H) spillover refers to the diffusion of activated hydrogen atoms from a hydrogen-rich activator such as transition metal catalysts to support materials with no ability to dissociate hydrogen molecules by themselves.[1-3] After its first discovery in the 1960s[4], many scientists have studied its fundamental aspects, as well as its utilization in applications for the design of advanced catalytic systems.[1, 2, 5-16] However, many aspects of H spillover are still veiled; particularly, one of the primary debates has centered on H spillover onto non-reducible metal oxide supports.[1]

Non-reducible support materials, such as alumina, silica, and zeolites, have commercial importance owing to their high thermochemical stability, renewability, tunable composition, adjustable acidity, and low cost.[17-19] However, H spillover onto non-reducible supports poses a difficulty in terms of understanding its mechanism. On a reducible support (semiconductors and conductors), H can migrate as a proton (H^+)/electron (e^-) charge pair instead of a H radical (H•) because the support is able to conduct e^- while the H^+ diffuses on the support surface. However, electron conduction is less feasible through non-reducible supports, leading to the consideration of the H migration mechanism mediated by H•.[1] According to the valence bond theory, H• is required to be coupled with another electron (with the opposite spin) of the support to form a strong covalent bond with a substantial binding energy, yielding undesirable kinetics for the migration.

Notably, our group has provided strong experimental evidence for the presence of H spillover over a zeolite surface, which is one of the non-reducible support materials.[20, 21] Using a model catalyst in which only H_2 is accessible to the zeolite-encapsulated Pt while preventing direct interaction between the organic molecule (e.g., benzene) and Pt, we showed that the benzene hydrogenation reaction could be catalyzed via mediation by the spilt-over H. To achieve a mechanistic understanding of the experimentally observed H spillover, we also proposed that the surface hydroxyl groups (e.g., Brønsted acid sites; BAS) could play a key role in relaying the spilt-over H on the zeolite surface based on density functional theory (DFT) calculations.

Although there have been several theoretical studies to provide a mechanistic insight on the H spillover over support surface such as zeolite, most of them have mainly focused on the local interaction between H atom and support surface or H transfer step between the support surface and the metal nanoparticle.[15, 16, 22, 23] This can be considered as 'hydrogenation' (or reduction) of supports. However, it should be pointed out that hydrogenation of supports may have little relevance for describing the catalytic usability of H spillover on the support surfaces. To thermodynamically drive the hydrogenation of the support, the chemical potential of H on the support should be lower than that on the metal surface. To utilize spilt-over H over the course of catalytic cycle, however, the chemical reaction of spilt-over H with another organic molecule provides a substantial thermodynamic driving force although the chemical potential of H on the support could be higher than that on the metal surface (i.e., not every elementary step has to be exothermic; rather elementary

[a] Graduate School of Energy, Environment, Water, and Sustainability (EEWS), Korea Advanced Institute of Science and Techn ology (KAIST), Yuseong-gu, Daejeon 305-701, Korea. E-mail: linus16@kaist.ac.kr (H. K.)
[b] Department of Chemical and Biomolecular Engineering, Korea Advanced Institute of Science and Technology (KAIST), Yuseong-gu, Daejeon 305-701, Korea.

† Electronic Supplementary Information (ESI) available: [Atomistic structures, reaction energy diagrams and diffusion constants]. See DOI: 10.1039/x0xx00000x

steps having the energetics of ΔE < ~1.3 eV can be responsible for the H spillover based catalytic cycle; *vide infra*). For getting insights on whether H spillover can be used for catalysis, therefore, the calculation should include full descriptions for the dissociation of H_2 on the metal cluster (e.g., Pt), the migration of activated H from the metal surface to the support surface (e.g., zeolite), the long-range diffusion of spilt-over H throughout the support surface and the chemical reaction of the spilt-over H with an organic molecule at the exterior surface of support crystallite.

With these regards, we performed extensive sets of DFT calculations to elucidate the mechanism of the entire catalytic process mediated by H spillover, using three different cluster models to describe Pt-zeolite interface, interior domain of zeolite crystallite, and zeolite external surface (terminal Al site is present as tri-coordinated form). To our knowledge, we note that this is the first theoretical work to deal with the entire H spillover based catalytic process.

2. Simulation details

2.1 Model systems

We considered the entire catalytic process using spilt-over H as a sequence of the following four steps[2, 24], as schematically shown in Fig. 1a:

I) activation of H_2 on the Pt surface,
II) migration of H atoms from the Pt surface to the adjacent zeolite surface (i.e., H spillover),
III) long-range diffusion of spilt-over hydrogen throughout the zeolite surface, and
IV) chemical reaction of the spilt-over hydrogen with the organic reactants (e.g., benzene) on the exterior surface of zeolite crystallite.

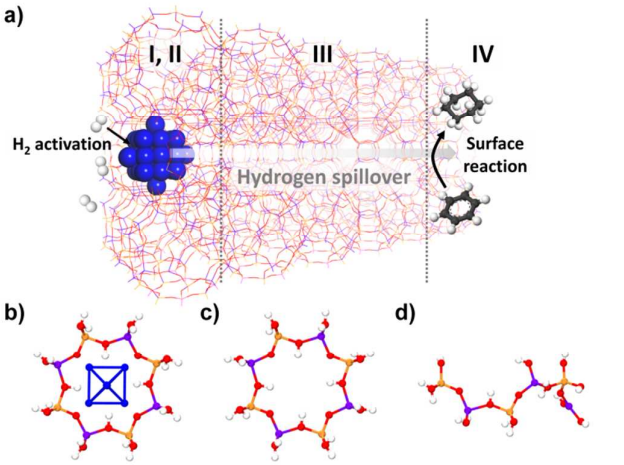

Fig.1. (a) Schematic representation of the entire hydrogen spillover pathway from a Pt cluster to a zeolite surface. (b) Pt_6 cluster coupled with a ring-shaped zeolite model (8T Al and Si atoms) to describe the H_2 activation (step I) and H spillover (step II) at the Pt-zeolite interface, (c) ring-shaped zeolite model (8T Al and Si atoms) to describe the H diffusion over the interior domain of a defect-free zeolite crystallite (step III-1), and (d) open linear chain model (6T Al and Si atoms) to describe the zeolite framework consisting of a nearby Lewis acidic defect site (LAS) for investigating H diffusion over the interior domain of a zeolite crystallite with LAS (step III-2) and chemical reaction of spilt-over H with organic molecules at the external zeolite surface (step IV). White, blue, orange, purple and gray represent H, Pt, Si, Al, and C atoms, respectively.

Considering the size dimensions of the zeolite crystallite, direct simulation of the above steps employing a single simulation model requires DFT calculations of several hundred nanometers, which is apparently beyond the capability of current computing technology. We thus investigated the entire reaction pathway at three different regimes using various model systems.

To examine steps I and II occurring at the Pt-zeolite interface, we employed a ring-shaped zeolite model consisting of 8T (Si and Al) atoms and interacting with a Pt_6 cluster (Fig. 1b). It is notable that similar models were used in previous studies on the reverse H spillover mechanism (which considered only the local H transfer from the zeolite surface to the metal nanoparticle).[25-30] To investigate step III occurring at the interior domain of the zeolite, we employed two different models; one is the ring-shaped structure of 8T (Fig. 1c) to represent a defect-free part of the zeolite framework, and the other is the linear chain structure of 6T (Si and Al) with one terminal trivalent Al site (Fig. 1d) to demonstrate the role of Lewis acidic defect sites (LAS). For the study of step IV occurring at the exterior surface, we used the same linear chain structure as in Fig. 1d to reflect the chemical condition of the zeolite external surface. It is of noted that our calculations showed that such LAS are inert upon the direct hydrogenation (associated free energy is uphill by 2.27 eV based on our DFT calculations), and thus abundant Lewis-acidic under-coordinated Al species are expected at the surface regime, which serve as active catalytic sites for the benzene hydrogenation. The initial atom positions of all considered zeolite models were obtained from the parts of the experimental NaA structure (ICSD 9326[31]), as shown in Fig. S1 in ESI†, composed of an alternative arrangement of Al and Si atoms obeying the Löwenstein rule[32] (Si/Al = 1). We saturated the dangling oxygen atoms generated while truncating a part of the model structure from the full zeolite crystal structure with hydrogen, and these oxygen atoms were fixed at their original positions from the experimental structure while all other atoms were fully relaxed during the DFT structural optimization. The bridge oxygen atoms between Al and Si were also hydrogenated to form a BAS, which is expected to be formed during the decationization step of the zeolite.[20] We also note that BAS of zeolite can be homolytically decomposed[33], which indicates their substantial radical-like characteristics and potential to be used as a mediator for migration of H.

2.2 Density functional theory (DFT) calculations

We calculated the DFT ground state energy at each reaction step by employing an M06-2X functional[34] combined with a LACVP** basis set.[35] All calculations were performed using the Jaguar 7.6 program.[36]

The ground state geometries were fully optimized under the geometric constraints explained in previous section of 2.1, and the transition states were optimized by following the

eigenvector of the Hessian matrix with the largest negative eigenvalue and were confirmed to have a single imaginary vibrational frequency. Mulliken charge and spin analyses[37] were performed to determine whether the character of the H atom was protonic or radical-like.

3. Results and discussion

3.1 H_2 activation (step I@Pt)

Using the Pt_6 cluster interacting with the zeolite model, as depicted in Fig. 1b, we calculated the DFT energetics during its sequential hydrogen chemisorption steps (Fig. S2 in ESI†). This analysis demonstrates that H_2 gas molecules can be continuously transferred to the Pt_6 cluster until it is saturated with 12 H atoms (Pt_6H_{12}). We note that the free energy of H_2 molecule is taken as the reference energy of the H atom. The average hydrogen molecule adsorption energy per H on the Pt cluster of 0.55 eV is comparable to that on the three-layer Pt (111) slab of 0.51 eV.[38]

3.2 H spillover from Pt to zeolite surface (step II@interface)

The last hydrogen chemisorption step of the Pt_6 cluster (Pt_6H_{11} + 1/2 H_2 → Pt_6H_{12}; ΔE = –0.63 eV; R1 in Fig. 2) is followed by the spillover of hydrogen from the Pt_6 cluster to the zeolite surface. To initiate H migration, we first considered the simultaneous generation of two defect sites, the H^+-deficient site of $[AlO_4]^-$ and the H^+-rich site of $[AlO_4H_2]^+$, via a proton rearrangement between the surface OH groups of the zeolite surface.[20] Near the Pt_6 cluster, our DFT result showed that this step is energetically favorable by ΔE = –0.27 eV along with the small activation energy of $\Delta E^{\ddagger}$ = 0.52 eV (R2 in Fig. 2). It is of noted that such an H transfer step to yield $[AlO_4]^-$ and $[AlO_4H_2]^+$ sites requires ~0.5 eV where no Pt nanoparticle exists nearby (vide infra). We found that the Pt_6H_{12} develops a specific interaction with the $[AlO_4]^-$ site (Fig. S3 in ESI†), which can ascribe the exothermic character for the H transfer in R2. Once the pair of defect sites is formed, the H species chemisorbed on the Pt_6 surface can migrate into the H^+-deficient $[AlO_4]^-$ site, which is a 1.40 eV uphill process (R3 in Fig. 2). Interestingly, at this step, Mulliken spin analysis indicated that the spilt-over hydrogen has a protonic character (spin = 0, charge = +0.43), which neutralizes the $[AlO_4]^-$ site by forming a surface OH group, while an electron remains in the Pt cluster (Mulliken charge of the Pt cluster is changed by –0.70). The long-range electrostatic attraction between the $[AlO_4H_2]^+$ site and the negatively charged Pt cluster is expected to stabilize the system.

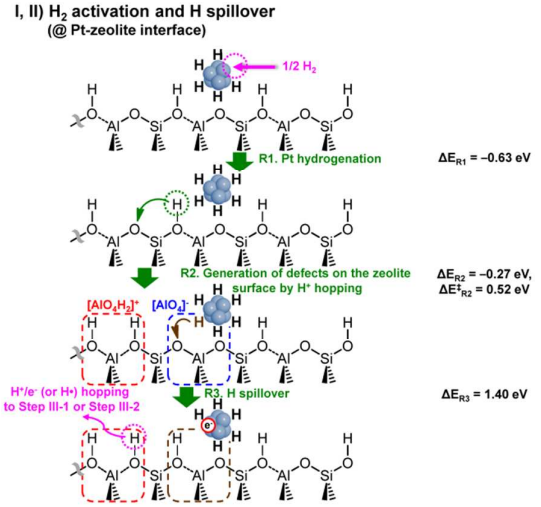

Fig. 2. Proposed reaction pathway and associated energy changes for steps I–II at Pt-zeolite interface where the H atom is activated and spilt-over from the Pt to the zeolite surface. Additional details are provided in Fig. S4 in ESI†.

3.3 H diffusion on the zeolite interior surface (step III@interior)

To discuss the long-range diffusion of spilt-over H on the zeolite interior surface, we initiated our mechanism by considering the simultaneous defect generations of a H^+-deficient $[AlO_4]^-$ site and H^+-rich $[AlO_4H_2]^+$ / $[AlO_3H]^+$ sites via proton rearrangement similar to that discussed in the previous section. In both models without and with the trivalent Al site (ring-shaped model in Fig. 1c and linear chain model in Fig. 1d), our DFT results showed that the generation of a defect pair is energetically and kinetically viable; defect generation in the ring-shaped model requires only ΔE = 0.49 eV with a barrier of $\Delta E^{\ddagger}$ = 0.98 eV (R1 of Fig. 3), and defect generation in the linear chain model requires ΔE = 1.05 eV with a barrier of $\Delta E^{\ddagger}$ = 1.26 eV (R1 of Fig. 4).

Therefore, at a finite temperature of ~500 K, such results suggest the presence of creation and annihilation dynamics at two defect sites with concentrations that are in dynamic equilibrium. Moreover, sequential proton rearrangements among surface OH groups can effectively diffuse the defect sites over a long range similar to the Grotthuss-type mechanism; successive proton hopping to diffuse defect sites requires ΔE = 0.06 eV with a barrier of $\Delta E^{\ddagger}$ = 0.79 eV for the ring-shaped model (R2 of Fig. 3), and ΔE = 0.47 eV with a barrier of $\Delta E^{\ddagger}$ = 1.09 eV for the linear chain model (R2 of Fig. 4). We further note that the proton has a strong quantum mechanical character such that it can tunnel through the energy barrier, expediting the proton rearrangement among surface OH groups.

We now consider the simultaneous defect generation at the zeolite interior regime, yielding $[AlO_4]^-$@interior and $[AlO_4H_2]^+$@interior/$[AlO_3H]^+$@interior, which is followed by their surface diffusion. By recalling that the $Pt_6H_{11}^-$ and $[AlO_4H_2]^+$ sites (which will be denoted as $Pt_6H_{11}^-$@interface and $[AlO_4H_2]^+$@interface, respectively) are formed at the final stage of the H spillover step (see the previous section 3.2 describing step II), the $[AlO_4]^-$@interior can eventually migrate near the $[AlO_4H_2]^+$@interface to annihilate both sites, which resultantly yields the long-range diffusion of the spilt-over H (to be exact, spilt-over proton) from the Pt-zeolite interfacial regime to the regime at which the $[AlO_4H_2]^+$@interior site is located. For the complete migration of H, however, the electron (e^-) localized at the $Pt_6H_{11}^-$@interface is eventually required to migrate to the zeolite interior regime as well as the

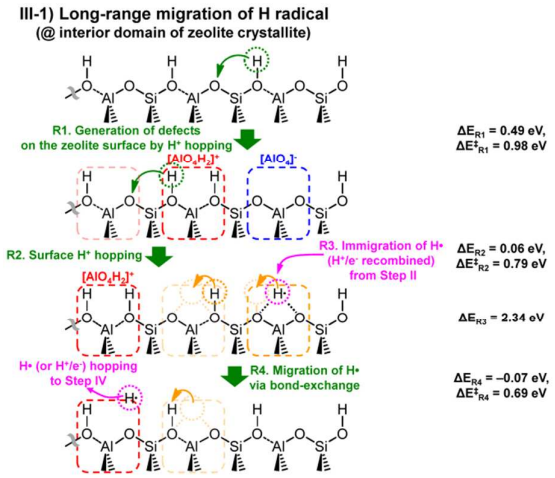

Fig. 3. Proposed reaction pathway and associated energy changes for step III at a defect-free zeolite interior surface (no LAS) where the spilt-over H immigrates from step II in the form of a H radical (H•) and diffuses via a bond-exchange mechanism. Additional details are provided in Fig. S5 in ESI†.

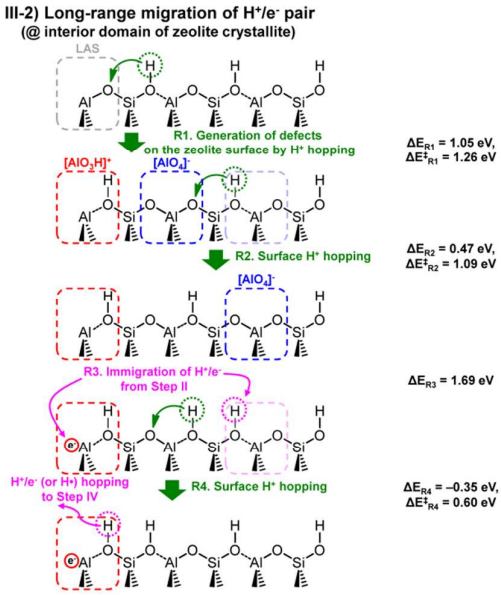

Fig. 4. Proposed reaction pathway and associated energy changes for step III at a zeolite interior surface with a nearby LAS where the spilt-over H immigrates from the step II in the form of a separate proton-electron (H^+-e^-) pair and diffuses via proton relay among surface hydroxyls. Additional details are provided in Fig. S6 in ESI†.

proton. Although a band transport of the electron is unavailable for the insulating zeolite, a hopping mechanism among possible localized states can provide an alternative pathway for the electron migration.

We thus considered a reaction step for immigrating a pair of H^+ and e^- from the Pt-zeolite interfacial regime to the zeolite interior regime over a long range, resulting in one H^+-rich $[AlO_4H_2]^+$ site with an additional e^- at the interior regime. The DFT results showed that this requires an energy cost of 2.34 eV for the ring-shaped model (R3 of Fig. 3); however, it is notable that the linear chain model requires only 1.69 eV of energy cost (R3 of Fig. 4). Such a dramatic energetic difference can be attributed to the different characteristics of the electron-localized state. By analyzing the DFT wavefunction, we found that the external trivalent Al acting as an LAS provides a good e^- accepting site where the additional e^- can be localized (Mulliken spin of Al atom changes from 0.00 to 0.90), whereas the H^+ is located on H^+-deficient $[AlO_4]^-$, forming a new surface OH.

For the ring-shaped model with no LAS, however, the additional e^- has no specific site at which to be localized, but it combines with the H^+ to form H· by forming a three-centered O-H-O bond. When the carrier of the spilt-over H develops the radical character of H· in the ring-shaped model, the surface proton hopping cannot further explain the H migration at the zeolite interior regime. As an alternative to the surface proton hopping, we can regard the three-centered O-H-O bond (where H· is located) as a local structural distortion from the conventional O-H bond of the surface hydroxyl group. We then consider the change of the adjacent O-H bond to the new three-centered O-H-O bond while recovering the original three-centered O-H-O to the O-H bond by simply rearranging bond connectivity. This effectively migrates the H· on the surface, which can be conceived as a polaron-type conduction mechanism.[20] DFT showed that the energy barrier for the polaron-type conduction is 0.69 eV (ΔE = –0.07 eV; R4 of Fig. 3).

When the carrier of the spilt-over H is H^+ while e^- is localized at an LAS (i.e., in the case of the linear chain model), further proton migration can be achieved via another successive surface proton rearrangement (R4 of Fig. 4, ΔE = –0.35 eV and $\Delta E^‡$ is 0.60 eV). We thus postulate the overall long-range electron hopping pathway from the Pt nanoparticle to the internal LAS to the catalytic active site located at the exterior regime while the proton diffuses via successive proton relay among surface OH groups. More discussions will be provided in the following sections.

3.4 Chemical reaction of spilt-over H at the zeolite exterior surface (step IV@exterior)

At the external surface of the zeolite crystallite, surface atoms usually exist as undercoordinated; in particular, Lewis-acidic tri-coordinated Al sites are expected. We thus examined the chemical reaction of the spilt-over H with the benzene using the linear chain model (Fig. 1d) where one tri-coordinated Al site exists.

DFT results showed that the external tri-coordinated Al site provides a good binding site for the unsaturated organic compound, yielding $C_6H_6^*$ (R1 of Fig. 5; ΔE = –0.81 eV); thus, the exposed LAS can serve as a catalytic active center for the hydrogenation reaction. With binding benzene at the LAS, the energetics for the simultaneous generation and migration of the $[AlO_4]^-$ and $[AlO_3H]^+$ sites are calculated as still feasible (R2 of Fig. 5: ΔE = 0.47 eV and $\Delta E^‡$ = 1.18 eV, and R3 of Fig. 5: ΔE = 0.39 eV and $\Delta E^‡$ = 1.06 eV). Thus, the $[AlO_4]^-$ and $[AlO_3H]^+$ sites are migratory via sequential proton hopping among surface OH groups, which can be responsible for the H^+ migration from the interior to the exterior regime of the zeolite.

Consequently, we considered a reaction step of immigrating a pair of H^+ and e^- from the zeolite interior regime to the zeolite exterior regime, resulting in the formation of an OH bond on the H^+-deficient $[AlO_4]^-$ site with an additional e^- at the exterior

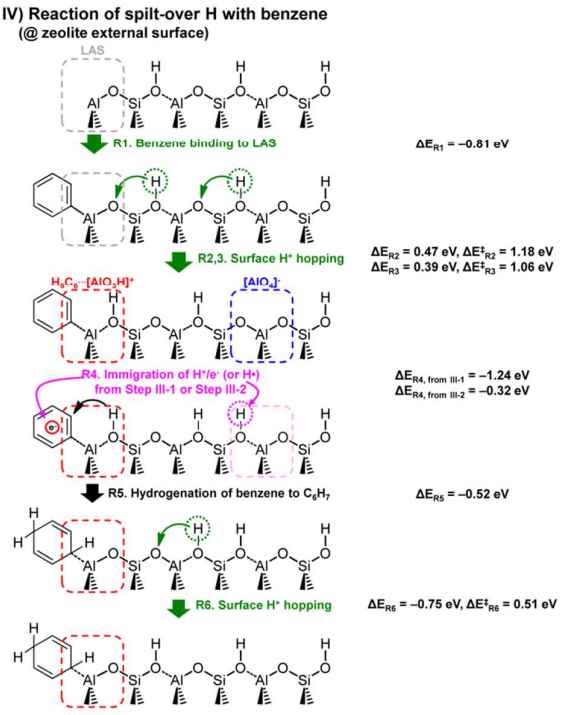

Fig. 5. Proposed reaction pathway and associated energy changes for step IV at zeolite exterior regime where the spilt-over H immigrates from step III in the form of a separate proton-electron (H^+-e^-) pair, diffuses via proton relay among surface hydroxyls, and then reacts with benzene at the surface LAS. Additional details are provided in Fig. S7 in ESI†.

regime (R4 of Fig. 5; ΔE = –1.24 eV or –0.32 eV, depending on whether the pair is transferred from the ring-shaped model or the linear chain model of the zeolite interior regime). Attributable to the presence of the LAS at the exterior regime, the e^- can be separately localized at the active center, which immediately reduces the adsorbed benzene, yielding $C_6H_6^{-*}$ (Mulliken spin of the benzene increases from 0.00 to 0.90 after the H^+/e^- immigration step), whereas the H^+ is bound to the zeolite surface as a surface OH group. Then, the H^+ located near the active site is transferred to $C_6H_6^{-*}$, resulting in the first hydrogenation of the benzene using spilt-over H (R5 of Fig. 5; ΔE = –0.52 eV). Further proton rearrangement recovers the original state of the surface OH groups (R6 of Fig. 5; ΔE = –0.75 eV and $\Delta E^{\ddagger}$ = 0.51 eV), enabling the successive hydrogenation reactions over the catalytic cycles. By repeating the analogous pathway, the second through sixth hydrogenations eventually convert benzene to cyclohexane, and the associated DFT energetics are shown in Fig. S8 in ESI†.

3.5 Entire H spillover pathway and role of different acid sites

Our proposed mechanism can be illuminated with the following key ideas: (1) H^+ is migratory among surface OH groups existing throughout the internal and external zeolite surface via a number of OH bond rearrangements (Grotthuss-like mechanism); (2) e^- is spatially localized either at the Pt nanoparticles, LAS at the interior regime, or LAS at the exterior regime (namely, e^- attractors) among which electron hopping is responsible for the electron migration; (3) at the regime where no e^--attractor exists nearby (which could be referred as a "defect-free regime"), H^+ and e^- are recombined to form H·, which is stabilized at the zeolite surface by forming a three-centered O-H-O bond that diffuses along the surface by converting the neighboring surface O-H bond into a three-centered O-H-O bond while restoring the original three-centered bond into a two-centered O-H bond (polaron-type mechanism). Therefore, over the course of the H spillover process, our mechanism considers the dynamic change of the spillover carrier between the H^+/e^- pair and H·, depending on the local chemical/electronic environment in which the carrier is located (Fig. 6a). Notably, Roland *et al.* also discussed that the H spillover should not be simply considered as a migration of an "invariable" chemical species. Rather, these researchers suggested that the possibility of dynamic equilibrium between the H^+/e^- pair and the H· should be considered, where their relative ratio depends on the electronic properties of the supports.[3] We think that our model suggests microscopic detail of the previously discussed dynamic equilibrium model for H spillover.[3]

The overall energetics throughout the proposed H spillover pathway and its catalytic participation are summarized in Fig. 6b. The energetically least favorable step is the H^+/e^- immigration step from the Pt-zeolite interfacial regime to the zeolite interior regime when the spillover carrier migrates through the "defect-free regime" with only a tetrahedral coordination of Si and Al (2.34 eV). However, the presence of an LAS (trivalent Al) in the interior domain can substantially lower the required energy up to 1.69 eV by enabling an H^+/e^- pair migration pathway (see Fig. 6 and compare the red and blue pathways). In the real sample, it should be noted that an LAS can exist in the interior domain of the zeolite owing to the presence of extra-framework Al generated during the zeolite synthesis and the decationization process.

Considering the transition state theory for the diffusion coefficient, $D = d^2\nu^* \exp(-E_{act.}/K_BT)$[39], the elementary step with the energetic barrier of < ~1.30 eV would be appreciable only for the diffusion over the long range for scales at tenths to thousands of nanometers (temperature $T \approx 523$ K, hopping distance $d \approx 3$ Å, and attempt frequency $\nu^* \approx 3700$ cm^{-1}, which is the range of OH vibrational frequencies[40, 41], were used for the estimation; see Table S1 in ESI† for details). Thus, the energy cost of 1.69 eV is still high. However, it should be noted that we assumed a one-step immigration of H^+/e^- from one fragment of the zeolite having the interaction with the Pt nanocluster to the other fragment of the zeolite where no Pt exists. Such a rough approximation is primarily due to the lack of the full atomistic modeling for the smooth change of the chemical environment from the Pt-zeolite interface regime to the zeolite interior regime, requiring unaffordable computational costs. We thus conceive that the H^+/e^- immigration step actually consists of multiple elementary steps during the continuous variation of the chemical environment from one regime to the other; thus, the barrier of each reaction step is expected to be much smaller. Next, the rate determining step will be switched to the H^+ migration step from the Pt nanoparticle to the zeolite surface (the DFT energy

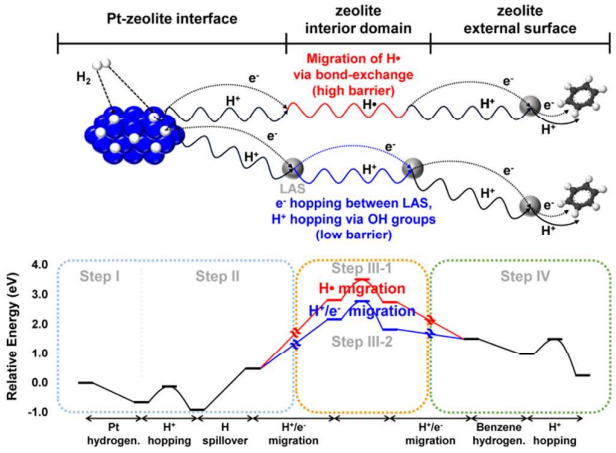

Fig. 6. When the zeolite crystallite contains substantial Lewis acid sites (LAS) connecting the internal domain and the external surface, spilt-over H migrates in the form of a H^+-e^- charge pair: H^+ hopping via surface OH groups (such as Brønsted acid sites; BAS) and e^- hopping between LAS. In the absence of LAS (i.e., defect-free regime), the spilt-over H is required to diffuse as a form of H radical (H•) by forming three-centered O-H-O bond. The bond-exchange between the O-H-O bond and the nearby surface O-H bond can transfer H radical over a long-range (polaron-type conduction). The H spillover step from the Pt to the zeolite surface requires a barrier of 1.40 eV, and the H migration step from the Pt-zeolite interface regime to the interior "LAS-free" domain of zeolite requires a barrier of 2.34 eV; the latter can be lowered by 0.65 eV when the interior domain of zeolite contains LAS, where e^- can be separately stabilized.

for this step is 1.40 eV, which would be less than it considering the possibility of the proton tunneling). However, more in-depth study and theoretical modeling of a detailed atomistic nature at this transition regime are necessary to complete the H spillover mechanism on the zeolite.

Our mechanism suggests the distinctive roles of different acid sites; the chain of surface OH groups such as BASs relay the H^+ for efficient migration whereas LASs expedite e^- migration and also act as activation sites for unsaturated reactant molecules (such as benzene). This explains our previous experimental observation that the catalytic activity is enhanced by one order of magnitude after the decationization process, which is attributable to the importance of surface OH groups.[20, 21] Our experimental results further demonstrated that mixing the decationized sample (where a sufficient number of surface OH groups is already developed in the zeolite) with other various physical diluents tunes the catalytic activity; mixing with more Lewis acidic diluents results in higher catalytic activity, which is consistent with our mechanism.[21]

4. Conclusions

To elucidate the entire hydrogen spillover mechanism and its catalytic participation, we performed a series of DFT calculations using fragmented model systems consisting of the essential chemical environment of the Pt-encapsulated zeolite system. On the basis of the DFT results from each model system, we proposed a H spillover mechanism covering the process from H_2 activation on a metal surface to its chemical reaction with organic molecules at the support surface.

There have been ongoing debates regarding the existence and catalytic functions of H spillover on non-reducible support materials such as zeolite owing to the lack of a comprehensive understanding of the H spillover mechanism. In terms of constructing a plausible H spillover mechanism, we must emphasize that the "support hydrogenation" and "catalytic function of H spillover during catalysis" should be differentiated (although both are often termed as H spillover[42]). The "support hydrogenation" accompanies appreciable reduction of the support surface by transferring a significant amount of H from the metal, and thus reducible support has been regarded as essential. However, even without detectable hydrogenation of the support surface, H spillover can still be used for various hydrogenation reactions if there is a "net migration" of H atoms. With the continuous supply of unsaturated organic reactants for catalytic hydrogenation, the bond-forming reaction between the organic reactants and the atomic hydrogen can provide the thermodynamic driving force for H spillover; thus, H spillover can still participate in the catalytic reactions even on non-reducible supports although its hydrogenation is endothermic.

In this respect, our study included the entire reaction pathway to the chemical reaction of spilt-over H instead of simply focusing on the local H transfer event between the support surface and the metal nanoparticle as in most previous simulation studies. Our proposed mechanism may not be sufficient and may require more elaboration to enclose the long-standing debates about H-spillover on non-reducible supports; however, we think that our study provides new insight for H^+/e^- migration on the zeolite surface, which well explains the key experimental observations to date. We further anticipate that our work will help to elucidate the hydrogen spillover mechanism on non-reducible supports and its application in advanced catalytic systems.

Acknowledgements

This work was supported by the Global Frontier R&D Program (2013M3A6B1078884) on Center for Hybrid Interface Materials (HIM) funded by the Ministry of Science, ICT & Future Planning.

Notes and references

1. R. Prins, *Chem Rev*, 2012, **112**, 2714-2738.
2. W. C. Conner and J. L. Falconer, *Chem Rev*, 1995, **95**, 759-788.
3. U. Roland, T. Braunschweig and F. Roessner, *J Mol Catal a-Chem*, 1997, **127**, 61-84.
4. S. Khoobiar, *Journal of Physical Chemistry*, 1964, **68**, 411-412.
5. F. Roessner and U. Roland, *J Mol Catal a-Chem*, 1996, **112**, 401-412.
6. S. Yook, H. Shin, H. Kim and M. Choi, *Chemcatchem*, 2014, **6**, 2836-2842.
7. H. Shin, S. Jung, S. Bae, W. Lee and H. Kim, *Environ Sci Technol*, 2014, **48**, 12768-12774.
8. S. S. Han, H. Kim and N. Park, *J Phys Chem C*, 2011, **115**, 24696-24701.
9. S. K. Beaumont, S. Alayoglu, C. Specht, N. Kruse and G. A. Somorjai, *Nano Lett*, 2014, **14**, 4792-4796.
10. L. Chen, A. C. Cooper, G. P. Pez and H. Cheng, *J Phys Chem C*,

2007, **111**, 18995-19000.
11. B. H. Li, W. L. Yim, Q. J. Zhang and L. Chen, *J Phys Chem C*, 2010, **114**, 3052-3058.
12. H. Nishihara, S. Ittisanronnachai, H. Itoi, L. X. Li, K. Suzuki, U. Nagashima, H. Ogawa, T. Kyotani and M. Ito, *J Phys Chem C*, 2014, **118**, 9551-9559.
13. G. M. Psofogiannakis and G. E. Froudakis, *J Phys Chem C*, 2009, **113**, 14908-14915.
14. G. M. Psofogiannakis and G. E. Froudakis, *J Am Chem Soc*, 2009, **131**, 15133-15135.
15. X. W. Sha, M. T. Knippenberg, A. C. Cooper, G. P. Pez and H. S. Cheng, *J Phys Chem C*, 2008, **112**, 17465-17470.
16. Z. Wang, F. H. Yang and R. T. Yang, *J Phys Chem C*, 2010, **114**, 1601-1609.
17. A. Corma, *Chem Rev*, 1995, **95**, 559-614.
18. D. W. Fickel, E. D'Addio, J. A. Lauterbach and R. F. Lobo, *Appl Catal B-Environ*, 2011, **102**, 441-448.
19. D. W. Fickel, J. M. Fedeyko and R. F. Lobo, *J Phys Chem C*, 2010, **114**, 1633-1640.
20. J. Im, H. Shin, H. Jang, H. Kim and M. Choi, *Nat Commun*, 2014, **5**.
21. S. Lee, K. Lee, J. Im, H. Kim and M. Choi, *J Catal*, 2015, **325**, 26-34.
22. F. H. Yang, A. J. Lachawiec and R. T. Yang, *J Phys Chem B*, 2006, **110**, 6236-6244.
23. M. N. Mikhailov, I. V. Mishin and L. M. Kustov, *Catal Lett*, 2009, **128**, 313-317.
24. C.-C. J. F., Ph. D., University of Massachusetts, 1986.
25. G. N. Vayssilov and N. Rosch, *Phys Chem Chem Phys*, 2005, **7**, 4019-4026.
26. G. N. Vayssilov, B. C. Gates and N. Rosch, *Angew Chem Int Edit*, 2003, **42**, 1391-1394.
27. R. C. Deka and S. Baishya, *Catal Today*, 2012, **198**, 110-115.
28. G. P. Petrova, G. N. Vayssilov and N. Rosch, *Chem Phys Lett*, 2007, **444**, 215-219.
29. E. A. I. Shor, V. A. Nasluzov, A. M. Shor, G. N. Vayssilov and N. Rosch, *J Phys Chem C*, 2007, **111**, 12340-12351.
30. R. C. Deka, A. Deka and A. Miyamoto, *Catal Lett*, 2009, **131**, 155-159.
31. V. Smith J and G. Dowell L, *Z. Kristallog*, 1968, **126**, 135.
32. W. Löewenstein, *Am Mineral*, 1954, **39**, 92-96.
33. M. J. Nash, A. M. Shough, D. W. Fickel, D. J. Doren and R. F. Lobo, *J Am Chem Soc*, 2008, **130**, 2460-2462.
34. Y. Zhao and D. G. Truhlar, *Theor Chem Acc*, 2008, **120**, 215-241.
35. P. J. Hay and W. R. Wadt, *J Chem Phys*, 1985, **82**, 299-310.
36. Jaguar; version 7.6, Schrödinger, LLC, New York, NY, (2009)
37. R. S. Mulliken, *The Journal of Chemical Physics*, 1955, **23**, 1833-1840.
38. G. W. Watson, R. P. K. Wells, D. J. Willock and G. J. Hutchings, *J Phys Chem B*, 2001, **105**, 4889-4894.
39. G. H. Vineyard, *Journal of Physics and Chemistry of Solids*, 1957, **3**, 121-127.
40. Q. Du, R. Superfine, E. Freysz and Y. R. Shen, *Phys Rev Lett*, 1993, **70**, 2313-2316.
41. A. Morita and J. T. Hynes, *Chem Phys*, 2000, **258**, 371-390.
42. M. Choi, S. Yook and H. Kim, *Chemcatchem*, 2015, **7**, 1048-1057.